ACS APPLIED MATERIALS & INTERFACES

Research Article

Cite This: ACS Appl. Mater. Interfaces 2019, 11, 47270−47278

www.acsami.org

Ultrasensitive Transmissive Infrared Spectroscopy via Loss Engineering of Metallic Nanoantennas for Compact Devices

Jingxuan Wei,[†,‡,∥] Ying Li,[†,∥] Yuhua Chang,[†,‡] Dihan Md. Nuruddin Hasan,[†,‡,§] Bowei Dong,[†,‡] Yiming Ma,[†,‡] Cheng-Wei Qiu,*[,†,‡] and Chengkuo Lee*[,†,‡]

[†]Department of Electrical and Computer Engineering, National University of Singapore, 117583 Singapore

[‡]Center for Intelligent Sensors and MEMS, National University of Singapore, 117608 Singapore

[§]Department of Electrical and Computer Engineering, Northsouth University, Plot, 15, Block B Kuril—NSU Road, Dhaka 1229, Bangladesh

Supporting Information

ABSTRACT: Miniaturized infrared spectroscopy is highly desired for widespread applications, including environment monitoring, chemical analysis, and biosensing. Nanoantennas, as a promising approach, feature strong field enhancement and provide opportunities for ultrasensitive molecule detection even in the nanoscale range. However, current efforts for higher sensitivities by nanogaps usually suffer a trade-off between the performance and fabrication cost. Here, novel crooked nanoantennas are designed with a different paradigm based on loss engineering to overcome the above bottleneck. Compared to the commonly used straight nanoantennas, the crooked nanoantennas feature higher sensitivity and a better fabrication tolerance. Molecule signals are increased by 25 times, reaching an experimental enhancement factor of 2.8×10^4. The optimized structure enables a transmissive CO_2 sensor with sensitivities up to 0.067% ppm^{-1}. More importantly, such a performance is achieved without sub-100 nm structures, which are common in previous works, enabling compatibility with commercial optical lithography. The mechanism of our design can be explained by the interplay of radiative and absorptive losses of nanoantennas that obeys the coupled-mode theory. Leveraging the advantage of the transmission mode in an optical system, our work paves the way toward cheap, compact, and ultrasensitive infrared spectroscopy.

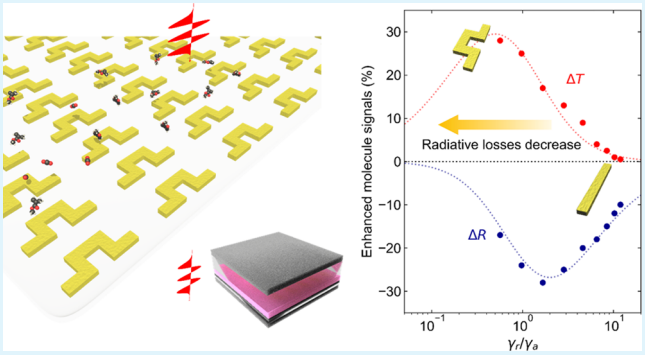

KEYWORDS: *nanoantennas, infrared spectroscopy, metamaterials, mid-infrared, coupled-mode theory*

1. INTRODUCTION

Infrared spectroscopy is a common technology for molecule detection with widespread applications in environment monitoring, chemical analysis, and biosensing.[1] Compared to other approaches, this technology provides valuable information on the characteristic absorption fingerprint of molecules, which is directly linked to their constituents, chemical bonds, and configuration. Consequently, an unambiguous, noninvasive, and label-free detection of substances is possible. However, due to the weak light−molecule interaction, conventional infrared spectroscopy, e.g., a nondispersive infrared sensor, usually suffers from bulky volume and slow response time.[2,3] To miniaturize infrared spectroscopy, one promising approach is nanoantennas, which can focus light into nanoscale volume with ultra-high field enhancement.[4−8] This is also known as surface-enhanced infrared absorption spectroscopy (SEIRA). In the past one decade, plasmonic nanoantennas with various structures and materials have been investigated,[9−13] and successful demonstration has been done in applications including chemical detection,[14−17] protein and lipid sensing,[18,19] monitoring of the structural change of molecules,[20] and chemical identification of single particle.[21]

However, the current nanoantenna designs are facing a trade-off between performance and fabrication cost, which limits a wider application of miniaturized infrared spectroscopy (see Supporting Information Section S1 for a summary of previous works). For example, most of the reported ultrasensitive devices leverage the strong mutual coupling of nanoantennas using nanogaps with a width of few nanometers.[21−23] In such nanogaps, the local electric field reversely scales with the gap width, and hence the light−molecule interaction will be increased.[24] So far, the state-of-the-art field enhancement is reported to be 10^7 in a sub-3 nm gap.[25] Unfortunately, the impressive enhancement factor (EF) is at the cost of complicated fabrication processes, which could be challenging for mass production via commercial cost-effective

Received: October 4, 2019
Accepted: November 26, 2019
Published: November 26, 2019

DOI: 10.1021/acsami.9b18002
ACS Appl. Mater. Interfaces 2019, 11, 47270−47278

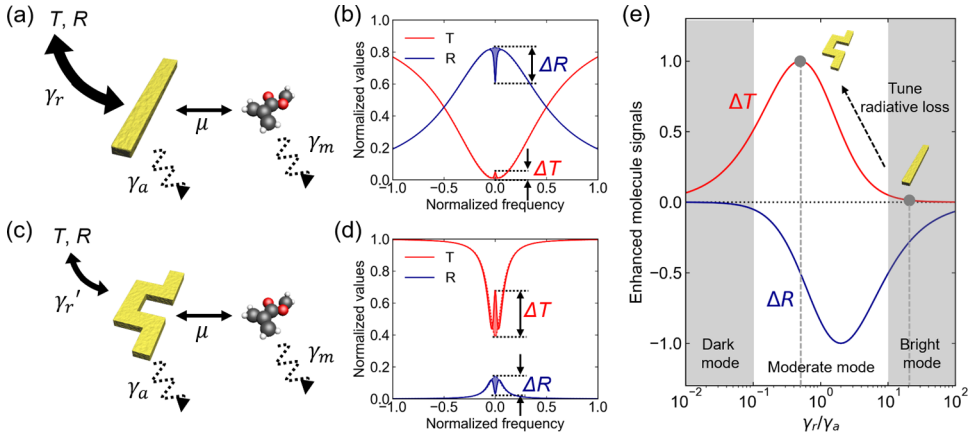

Figure 1. Design principle of transmissive infrared sensors based on crooked nanoantennas. (a, c) Modeling of straight and crooked nanoantennas, coupled with molecules. T and R represent transmission and reflection spectra. γ_r and γ_a denote the radiative and absorptive losses of nanoantennas, while γ_m is the absorptive loss of molecules. μ represents the coupling strength. The main difference between the two structures is the smaller γ_r in crooked nanoantennas. (b, d) Modeled transmission and reflection spectra for straight and crooked nanoantennas, with (solid curves) and without (dashed curves) coupling with molecules. The shaded areas represent the spectral difference induced by the existence of molecules. The height of shaded areas, ΔT and ΔR, denote the enhanced molecule signals in transmission and reflection spectra, respectively. (e) Derived dependence of the enhanced molecule signals on the radiative and absorptive losses of nanoantennas, under the conditions of no spectral detuning between the resonances of nanoantennas and molecules.

optical lithography. Besides, another two notorious drawbacks of these nanogaps are the reduced sensing area, which is roughly equal to the size of hot spots, and long response time due to poor accessibility. The problem in accessibility will require additional challenging techniques, e.g., integration with nanofluidics.[26] In addition to nanogaps, another common approach for higher sensitivity is to undercut the metallic structure so that the overlap between light and molecules is larger.[27] However, this improvement in performance is also at the cost of more challenging fabrication techniques. The trade-off is not only limited in the structure design but also in the choice of the operation mode. In infrared spectroscopy, there are two main operation modes, i.e., transmission and reflection modes. Practically, the reflection mode can achieve higher field enhancement by the use of a back reflector,[25] but it requires complex and bulky optical components to steer the light path, impeding its application for cost-effect compact devices. On the other hand, the transmission operation mode enables easy integration with a light source and a photodetector in a sandwich configuration, but it theoretically allows light to decay in both transmission and reflection channels, which may lead to a relatively low performance.[12] To solve the above issues, a new paradigm should be developed, which requires a deep understanding of nanoantenna-assisted infrared spectroscopy.

In this work, we present novel crooked nanoantennas to implement ultrasensitive transmissive plasmonic molecule sensors, based on loss engineering of nanoantennas. Although the concept of loss engineering has been reported in previous works on metamaterials,[28−32] it has not been experimentally applied in transmissive infrared spectroscopy. First, we establish a complete theoretical framework of this coupled system using the coupled-mode theory. Second, guided by theoretical analysis, we propose crooked nanoantennas with reduced radiative losses, demonstrating an enhancement factor of 2.8×10^4. This is about 25 times higher than the commonly used straight nanorod antennas. The measured results are well matched with our theory. Third, we also investigate the effect of nonzero spectral detuning between plasmonic and vibrational modes, when Fano resonance plays an important role. Fourth, we demonstrate a transmissive plasmonic CO_2 sensor based on optimized crooked nanoantennas with sensitivities up to 0.067% ppm^{-1}, which is 13 times higher than the straight nanorod antennas. Finally, we also investigate the higher-order modes of crooked nanoantennas and present multiband plasmonic sensors to simultaneously detect the refractive index and characteristic absorption of molecules. Our work opens a new avenue to achieve transmissive infrared spectroscopy with high performance and low cost, moving one further step toward compact, portable, and sensitive molecule sensors.

2. RESULTS AND DISCUSSION

2.1. Theoretical Analysis. The design principle of our approach to ultrasensitive transmissive plasmonic molecule sensors is illustrated in Figure 1. In conventional nanorod antennas, as shown in Figure 1a, the radiative loss (γ_r) is usually dominant over the absorptive loss (γ_a), which will theoretically lead to much smaller molecule signals in the transmission spectra (ΔT) than that in the reflection spectra (ΔR), as shown in Figure 1b. To optimize the transmissive signals, the γ_r can be reduced by crooking the nanoantennas (Figure 1c,d). As predicted by our theoretical analysis, the improvement factor achieved by our approach can be above one order, as shown in Figure 1e.

The significant improvement in our structure can be understood by modeling the plasmonic molecule sensors with the coupled-mode theory. In the following, we will highlight the key steps in theoretical analysis. As the starting point, we write the general equations of the coupled-mode theory[33]

$$\frac{\mathrm{d}}{\mathrm{d}t}P = j\omega_0 P - (\gamma_r + \gamma_a)P + j\mu M + \sqrt{\gamma_r}s_{in} \quad (1)$$

$$\frac{\mathrm{d}}{\mathrm{d}t}M = j\omega_m M - \gamma_m M + j\mu P \quad (2)$$

$$s_t = s_{in} - \sqrt{\gamma_r}Ps_r = \sqrt{\gamma_r}P \quad (3)$$

DOI: 10.1021/acsami.9b18002
ACS Appl. Mater. Interfaces 2019, 11, 47270−47278

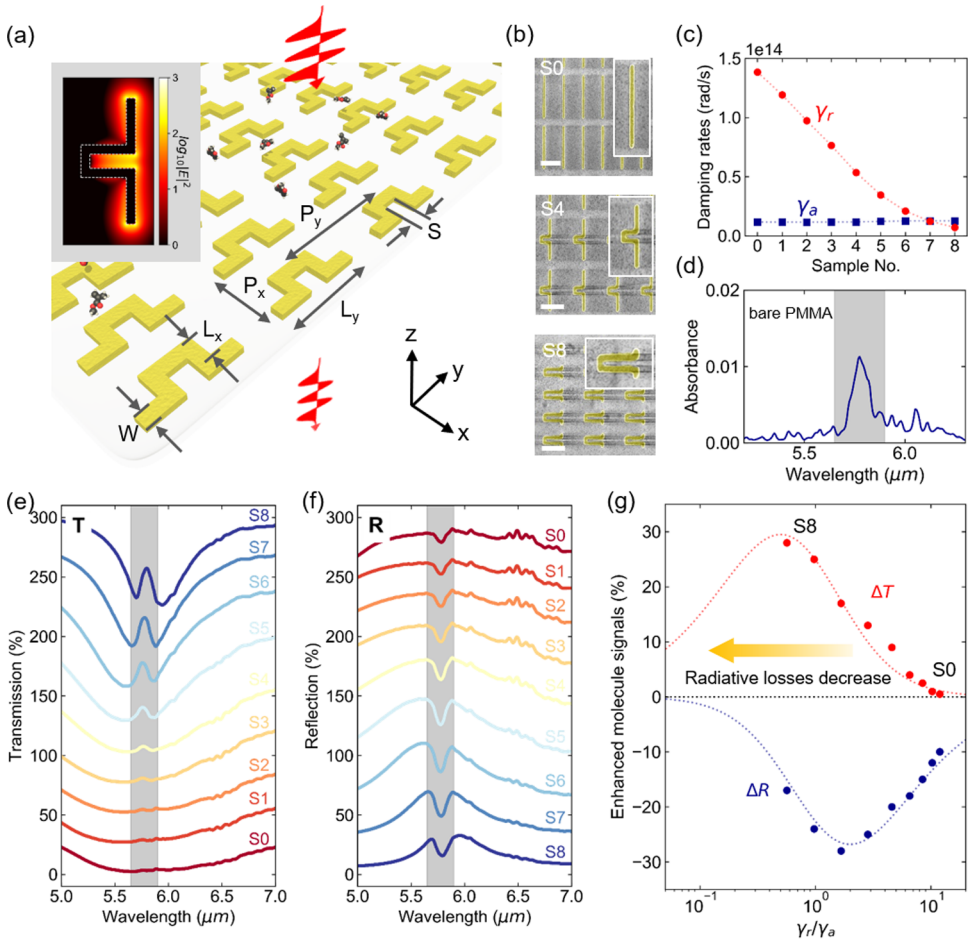

Figure 2. Proposed crooked nanoantennas and experimental results with no spectral detuning. (a) Schematic of transmissive infrared spectroscopy using crooked nanoantennas. The inset shows the simulation of the enhanced electric field due to the plasmonic resonance of nanoantennas. The polarization of incident light is along the *y*-direction. (b) Electron scanning microscopy images of three examples of designed samples with different folding degrees. False color has been used for better clarity. The scale bars are 1 μm. (c) Extracted radiative and absorptive damping rates of the designed samples. (d) Absorptance spectra of the thin poly(methyl methacrylate) (PMMA) layer as a reference. Gray shaded area denotes the bandwidth of characteristic molecular vibration in PMMA. (e, f) Measured transmission and reflection spectra of designed samples, coated with the 20 nm PMMA layer. The spectra are shifted vertically for clarity. (g) Measured dependence of the enhanced molecule signals on the radiative and absorptive losses of nanoantennas. Dashed lines show the theoretical prediction.

$$T = \left|\frac{s_t}{s_{in}}\right|^2 \quad R = \left|\frac{s_r}{s_{in}}\right|^2 \tag{4}$$

where P and M are the amplitudes of plasmonic and vibrational modes, respectively. ω_0 and ω_m represent the resonance frequencies of plasmonic and vibrational modes, respectively. γ_r and γ_a denote the radiative and absorptive losses of nanoantennas, while γ_m is the absorptive loss of molecules. μ represents the coupling strength. T and R denote transmission and reflection spectra, which are related to the amplitude of incident light (s_{in}), transmitted light (s_t), and reflected light (s_r). By substituting eqs 1−3 into eq 4 and replacing d/dt with $j\omega$, we obtain the far-field spectra for a given frequency of incident light (ω)

$$T(\omega), R(\omega) = \left|\frac{j(\omega-\omega_0) + \gamma_{a,r} + \frac{\mu^2}{j(\omega-\omega_m)+\gamma_m}}{j(\omega-\omega_0) + (\gamma_a+\gamma_r) + \frac{\mu^2}{j(\omega-\omega_m)+\gamma_m}}\right|^2 \tag{5}$$

Note that T and R contain a different term (γ_a for T, and γ_r for R) in the numerator. In practical, the enhanced molecule signals are expressed as the spectral difference of nanoantennas that is induced by coupling with the molecules

$$\Delta T = T - T|_{\mu=0} \tag{6}$$

$$\Delta R = R - R|_{\mu=0} \tag{7}$$

As we can see, the expression of the enhanced molecule signals could be very complicated. To acquire relatively simple analytical results, we will adopt several assumptions in our following derivation. First, we assume that $\omega = \omega_0 = \omega_m$. This condition is reasonable since the highest performance of plasmonic sensors is usually achieved when the two modes are aligned.[34−36] Second, we assume a weak coupling condition (μ is very small compared to γ_r and γ_a). Then, we can obtain the expressions of the enhanced molecule signals

$$\Delta T = \frac{2\gamma_a\gamma_r}{(\gamma_a+\gamma_r)^3}\frac{\mu^2}{\gamma_m} \tag{8}$$

DOI: 10.1021/acsami.9b18002
ACS Appl. Mater. Interfaces 2019, 11, 47270−47278

$$\Delta R = \frac{-2\gamma_r^2}{(\gamma_a + \gamma_r)^3}\frac{\mu^2}{\gamma_m} \quad (9)$$

From the equations, we can see that ΔT is positive while ΔR is negative, indicating that coupling with molecules will lead to peaks in the transmission spectra, but dips in the reflection spectra of nanoantennas. Besides, the expressions of ΔT and ΔR are obviously different, and the relative value $|\Delta T/\Delta R|$ is simply equal to $|\gamma_a/\gamma_r|$. In the case of bright modes where γ_r is much larger than γ_a, $|\Delta T|$ will be much smaller than $|\Delta R|$. In contrast, $|\Delta T|$ will become larger than $|\Delta R|$ in dark modes.

The derived expressions of the enhanced molecule signals in transmission spectra offer us a new dimension in the design space of plasmonic molecule sensors. Guided by our analysis, we can tune the radiative or absorptive losses of nanoantennas to optimize the molecule signals. Note that the absorption of nanoantennas is due to Ohmic loss, which is relatively robust against structural changes. We may be able to tune the radiative loss of nanoantennas by folding the structure while keeping the absorptive loss almost constant. This is also confirmed by our results later. In this case, we can relate the enhanced molecule signals with the normalized radiative loss ($f = \gamma_r/\gamma_a$) as

$$\Delta T \propto \frac{f}{(1+f)^3} \quad (10)$$

$$\Delta R \propto \frac{f^2}{(1+f)^3} \quad (11)$$

As shown in Figure 1e, the ΔT and ΔR reach their extremes when γ_r/γ_a equal 0.5 and 2, respectively. To implement plasmonic molecule sensors with maximum sensitivities, we should design nanoantennas in a moderate mode.

2.2. Experimental Realization. The schematic of our design for transmissive infrared spectroscopy is shown in Figure 2a. Our device consists of a nanoantenna array deposited on the CaF_2 substrate ($n = 1.4$), which is transparent in the mid-infrared range. Under infrared illumination with polarization along the y-axis, the plasmonic modes in nanoantennas will be excited, leading to the above two-order enhancement of the near-field intensity. When molecules are at the vicinity of nanoantennas, its interaction with light will then be boosted, leading to enhanced molecule signals that can be measured in the transmission spectra. As we have discussed, the enhanced molecule signals are strongly dependent on the radiative and absorptive losses of nanoantennas. To achieve the highest performance, we can tune the radiative loss to the optimal conditions by crooking the originally straight structure. In our experiments, we have designed nine samples, labeled from S0 to S8, with different folding degrees, and the scanning electron micrographs of three typical examples are shown in Figure 2b. The scale bars are 2 μm. The samples are fabricated using standard electron beam lithography followed with thermal deposition of 5:80 nm Ti/Au and a lift-off process. Detailed information, including structures and scanning electron microscopy images, can be found in the Supporting Information Section S2. As we can see, the effective length of nanoantennas along the polarization direction decreases from S0 to S8, suggesting gradually reduced radiative losses. This intuitive understanding is also confirmed by the extraction of γ_r and γ_a in the coupled-mode theory from the simulated transmission spectra, as shown in Figure 2c (see the Supporting Information Section S3 for the details). From the graph, the γ_r decreases from 1.38×10^{14} rad s^{-1} for S0 to 7.1×10^{12} rad s^{-1} for S8, while the γ_a only slightly changes from 1.16×10^{13} rad s^{-1} for S0 to 1.26×10^{13} rad s^{-1} for S8. The slight increase of γ_a could be because of the increased inductive self-coupling in the structure. Therefore, we have obtained a series of nanoantennas with similar γ_a, and tunable values of γ_r/γ_a from 11.9 (S0) to 0.56 (S8), which allows us to optimize the performance of transmissive plasmonic molecule sensors.

The fabricated nanoantenna samples are then coated with a 20 nm poly(methyl methacrylate) (PMMA) layer for sensing demonstration. PMMA is a model material with a distinct absorption peak around 5.8 μm due to the vibrational mode of C═O bonds, as shown in Figure 2d. The thickness of the PMMA layer is measured by atomic force microscopy (Supporting Information Section S4). The transmission and reflection spectra are measured by an integrated Fourier transform infrared microscope (Agilent Cary 620), and the results are shown in Figure 2e,f. The spectra have been shifted vertically for clarity. Gray shades denote the bandwidth of vibration modes of PMMA molecules. By measuring the height of transmission peaks and reflection dips, we can extract the enhanced molecule signals (ΔT and ΔR) for different samples. The measured molecule signals of 20 nm PMMA (495 K molecular weight) reach 28% in transmission spectra for S8. Note that the signals are mainly contributed by the molecules in the vicinity of nanoantennas. The sensitivity of our device (S8) can be calculated to be around 1% for 205 molecules per nanoantenna, corresponding to an enhancement factor of 2.8×10^4. The enhancement factor (EF) is calculated through $EF_{SEIRA} = (\Delta T_{SEIRA}/V_{SEIRA})/(\Delta T_0/V_0)$, where ΔT_{SEIRA} is the enhanced molecule signals measured from a nanoantenna enhanced sensor, ΔT_0 is the measured molecule signals from a bare CaF_2 substrate covered with the PMMA layer. V_{SEIRA} is the volume of PMMA molecules that occupies the hot spot at the surface of nanoantennas and contributes to infrared signals. V_0 is the volume of PMMA molecules coated on a bare CaF_2 substrate. The area of the hot spot for crooked nanoantennas (S8) is estimated to be around 2000 nm^2, by calculating the hot spot area at the nanoantenna tips, in which the width of the evanescent field has been assumed to be 10 nm. Obviously, we can see that the measured molecule signals increase significantly from S0 to S8. Figure 2g shows the measured ΔT and ΔR in all of the samples as a function of the corresponding γ_r/γ_a. The experimental results are well matched with our theoretical predictions. The nonmonotonous curves for transmission and reflection measurement confirm the mechanism to be loss engineering rather than field enhancement. Compared to the conventional nanorod antennas (S0), the optimized crooked nanoantennas (S8) show a larger ΔT with about 25 times improvement. Importantly, unlike previous efforts to achieve higher sensitivity by creating nanogaps with a smaller width, the improvement in our structure comes from the optimized conditions by engineering the losses of nanoantennas. Since our approach excludes sub-100 nm structures, we can leverage the commercial optical lithography for the mass production of our design. Therefore, our experiments have unambiguously confirmed the superiority of crooked nanoantennas over straight nanorod antennas, especially in the transmission mode.

2.3. Different Effects of Spectral Detuning on Straight and Crooked Nanoantennas. In the above theoretical and experimental demonstration, the spectral

DOI: 10.1021/acsami.9b18002
ACS Appl. Mater. Interfaces 2019, 11, 47270−47278

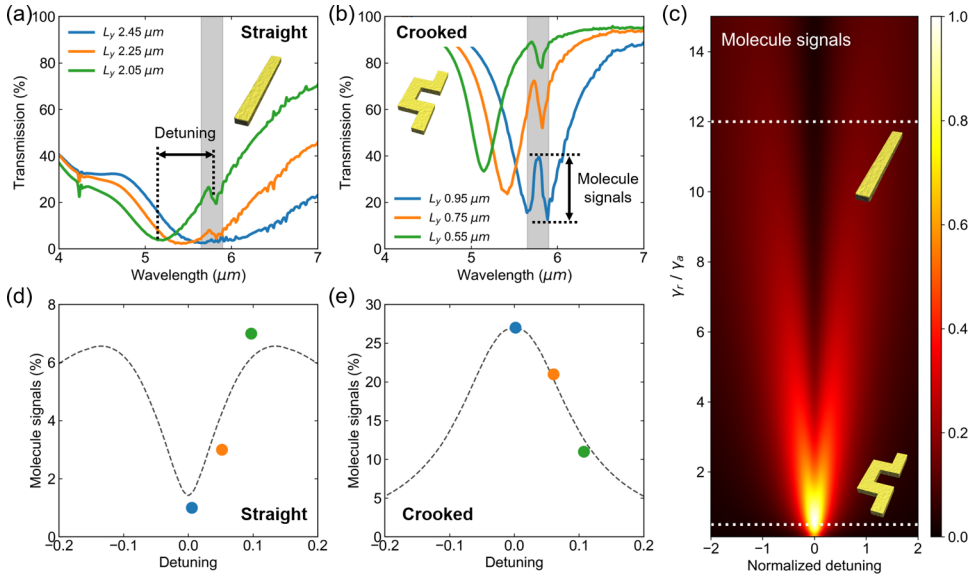

Figure 3. Effect of spectral detuning. (a, b) Measured transmission spectra for straight and crooked nanoantennas with different L_y as indicated, coated with a 20 nm PMMA layer. (c) Calculated two-dimensional mapping of enhanced molecule signals as a function of normalized spectral detuning and γ_r/γ_a. Two white dashed lines are the parameters of fabricated straight and crooked nanoantenna. (d, e) Measured molecule signals for straight and crooked nanoantennas as a function of spectral detuning, fitted with theoretical predictions.

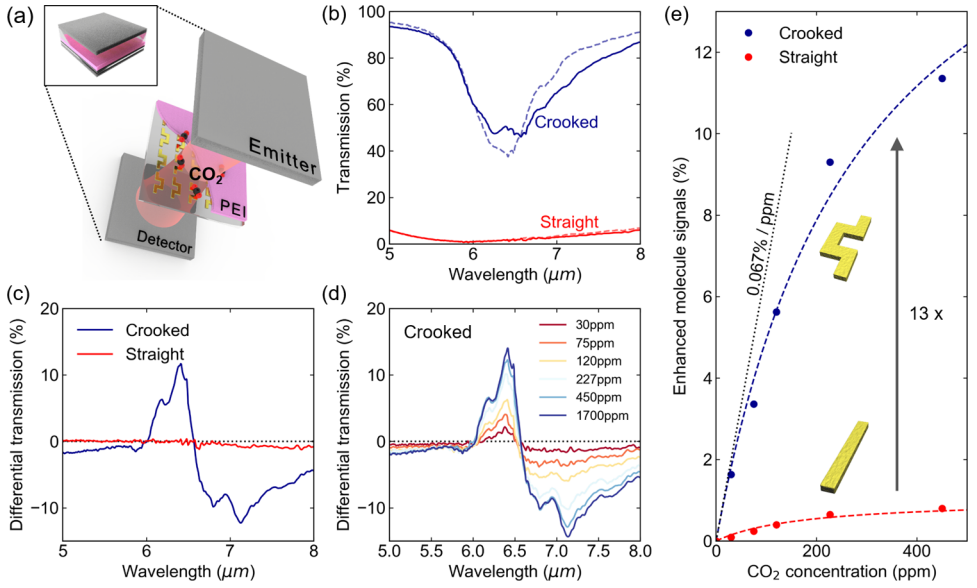

Figure 4. Demonstration of a transmissive CO_2 gas sensor. (a) Schematic of the transmissive CO_2 gas sensor. The inset shows an envisioned version of the compact sensing device. PEI is an enrichment layer, which adsorbs CO_2 molecules through reversible chemical reactions. (b) Measured transmission spectra of crooked and straight nanoantennas in nitrogen (broken lines) and ambient (solid lines) environment, respectively. (c) Baseline corrected results for nanorods and folded nanoantennas. (d) Baseline corrected results of crooked nanoantennas at different CO_2 concentrations. (e) Experimentally enhanced molecule signals versus the CO_2 concentration. Dashed lines show the fitting curves, and the dotted line shows the sensitivity of this sensor at low concentrations.

detuning between the resonance frequencies of plasmonic and vibration modes has been kept to be zero ($\omega_0 - \omega_m = 0$). We further investigate the effect of nonzero spectral detuning on both straight and crooked nanoantennas, as shown in Figure 3. By changing the L_y of nanoantennas, we can tune the resonance wavelength of the plasmonic mode, as shown in Figure 3a,b. When the detuning is not zero, we can clearly see that the transmission peaks become asymmetric or even transmission dips, which are typical features of Fano resonance.[37,38] The Fano resonance emerges because the contribution of molecular vibration to the plasmonic resonance becomes complex due to the spectral detuning. In this case, the molecule signals will be defined as the contrast between the peaks and dips. Although it is difficult to express the molecule signals in certain analytical formulas, numerical calculation can be conducted using eqs 5−7.

The calculated result of molecule signals is plotted against the detuning and γ_r/γ_a in Figure 3c. From the graph, we can conveniently find the optimal conditions of nanoantenna structures for transmissive plasmonic molecule sensors, which would be very useful for practical applications. Globally, there is only one maximum of molecule signals, where the plasmonic

DOI: 10.1021/acsami.9b18002
ACS Appl. Mater. Interfaces 2019, 11, 47270−47278

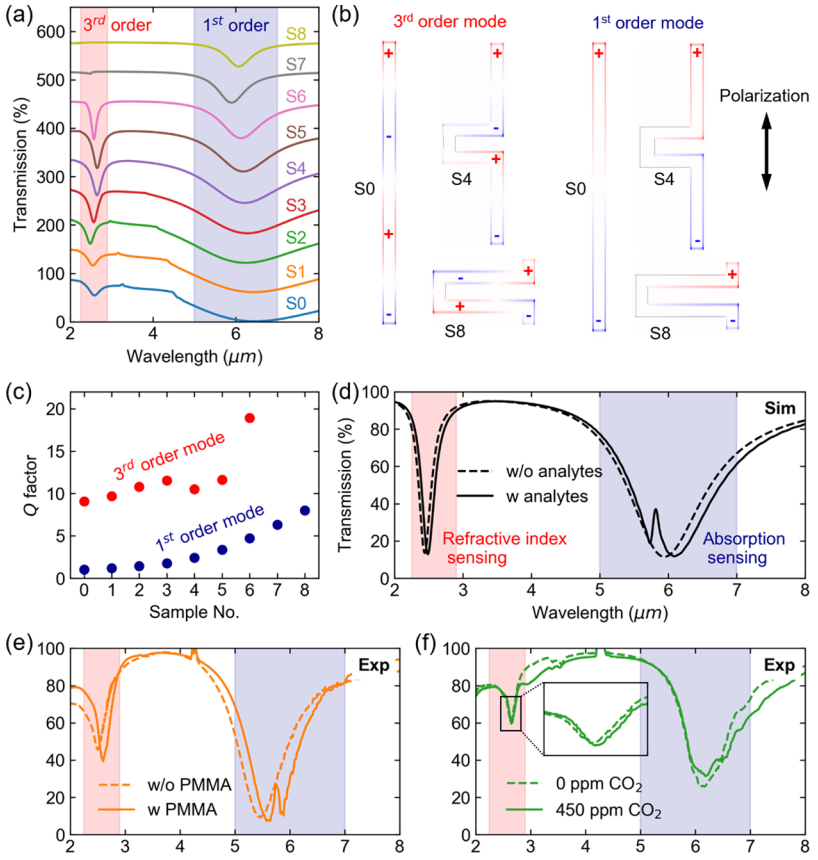

Figure 5. Higher-order modes in crooked nanoantennas. (a) Simulated transmission spectra of designed samples, in which the dips around 2.5 μm are due to the third-order mode of nanoantennas. The spectra are shifted vertically for clarity. (b) Simulated surface charge distribution of the designed nanoantennas at the first- and the third-order mode. The overall dipole moment along the polarization direction is roughly proportional to the radiative loss of nanoantennas. (c) Extracted quality (Q) factors of the first and the third resonance modes of designed nanoantennas. (d) Simulated transmission spectra of crooked nanoantennas (S6) with and without analytes. (e, f) Measured transmission spectra of crooked nanoantennas (S6) for sensing of a 20 nm PMMA layer and CO_2 gas. The wavelength shift in the inset is about 10 nm.

nanoantennas should be designed such that $\gamma_r/\gamma_a = 0.5$ and $\omega_0 - \omega_m = 0$. Any variation from the optimal conditions will lead to smaller molecule signals, that is, less sensitive molecule sensors. This rule should be general and applicable to other nanoantenna structures. However, we also observe an interesting phenomenon that there are two local maxima for bright plasmonic modes, for example, in nanorod antennas. Surprisingly, the two local maxima are achieved when the spectral detuning is nonzero. This is in sharp contrast to the conventional perception that the measured molecule signal is achieved at zero detuning, where the near-field intensity of plasmonic nanoantennas is maximum.[39] By fitting our experimental results as in Figure 3d,e, the different effects of spectral detuning on straight and crooked nanoantennas are clearly seen. The normalized detuning is defined as $(\lambda - \lambda_0)/\lambda_0$, where λ is the wavelength of the incident light. The fitting process can be found in Supporting Information Section S5. Note that at nonzero spectral detuning, the molecule absorption cannot be regarded as a pure absorptive load, Fano resonance should play a role in this anomalous effect of spectral detuning. However, a comprehensive understanding of this effect requires further investigation in the future.

2.4. Demonstration of Transmissive CO_2 Gas Sensor. After theoretically and experimentally validating the importance of loss engineering of plasmonic nanoantennas for molecule detection, we further demonstrate a transmissive CO_2 gas sensor based on the optimized crooked nanoantennas. As shown in Figure 4a, the proposed plasmonic sensor consists of metallic nanoantennas on CaF_2 chips coated with the thin polyethylenimine (PEI) layer,[40,41] which can be conveniently integrated with the light source and photodetectors due to the transmission operation mode, forming a compact molecule sensing device. As an enrichment layer, PEI is a polymer with amine groups, which can adsorb CO_2 molecules through reversible chemical reactions (see Supporting Information Section S6 for more details).[42,43] Once CO_2 is adsorbed in PEI, multiple vibration modes will emerge with the resonance wavelength from 6.0 to 7.7 μm. Because of the dynamic equilibrium established by the reversible chemical reactions, the CO_2 concentration in the environment can be conveniently monitored through the strength of the emerging characteristic absorption in the PEI layer. The thickness of the PEI layer in our device is around 150 nm. Figure 4b shows the measured transmission spectra in nitrogen (0 ppm, dashed lines) and in the ambient (450 ppm, solid lines) environment. In our experiment, the samples are placed in a gas cell, in which the CO_2 concentration is calibrated by a commercial CO_2 meter. After coating the PEI layer, the resonance wavelengths of straight (S0) and crooked (S8) nanoantennas are red-shifted to 6.0 μm and 6.4 μm respectively, due to the existence of the PEI layer. When the gas cell is filled with 450 ppm CO_2, we can see a significant change in the transmission spectra of crooked nanoantennas, while the change for straight antennas is only slight.

DOI: 10.1021/acsami.9b18002
ACS Appl. Mater. Interfaces 2019, 11, 47270−47278

To have a clear comparison, we plot the transmission difference of the two samples induced by 450 ppm CO_2, as shown in Figure 4c. From the graph, we can also see that the overall differential transmission of crooked nanoantennas is much larger than that of straight nanoantennas. Interestingly, for the crooked nanoantennas, we obverse a positive transmission difference between 6 and 6.5 μm wavelength, but negative transmission difference in the other range. Since the refractive index change in PEI due to CO_2 adsorption is small,[40] we attribute this phenomenon to the effect of spectral detuning as discussed above. To characterize the sensitivity of our design, we measure the differential transmission of crooked nanoantennas for different CO_2 concentrations from 30 to 1700 ppm, as shown in Figure 4d. The measured results indicate that our structure is most sensitive at low concentrations but will saturate gradually at high concentrations. The saturation at high concentrations is due to the limited accommodation sites for CO_2 molecules in PEI. To have a clear feeling of the concentration-dependent sensitivity, we plot the peak differential transmission against the CO_2 concentrations as Figure 4e. The trends can be well fitted with the derived function $\Delta T = \Delta T_0 - \Delta T_0/(1 + g n_{CO_2})$, where T_0 and g are fitting parameters (see Supporting Information Section S7 for detailed derivation). The fitted T_0 and g are 19.2% and 0.00348 ppm^{-1} for the crooked nanoantennas, but 1.0% and 0.00571 ppm^{-1} for the straight nanoantennas. The maximum sensitivity of the crooked nanoantennas at a low concentration limit can be calculated to be about 0.067% ppm^{-1}, which is about 13 times higher than the straight nanorod antennas. Considering the ultrathin thickness of our device, our sensor enables compact integration and fast response even for molecule detection in the nanoscale range.

2.5. Multiband Resonance in Crooked Nanoantennas. Multiband resonance in plasmonic nanoantennas provides opportunities for multifunctional molecule sensors, including complex refractive index sensing and simultaneous detection of different analytes.[6,16,44] Usually, the multiband resonance is realized by fabricating different plasmonic structures in one supercell, which may lead to complicated design and reduced light−matter interaction. In contrast, the loss engineered crooked nanoantennas can support tailorable multiple resonances in one single structure. Figure 5a shows the simulated transmission spectra, indicating the transmission dips attributed to the first and the third-order modes. In our discussion above, we have been using the first-order mode around 6 μm for sensing demonstration. Besides, from the graph, we can see narrow dips around 2.5 μm in S0−S6, which are attributed to the third-order mode. Note that the second-order mode is forbidden due to its symmetry. Figure 5b shows the surface charge oscillation of the two modes. In terms of the first-order mode, the nanorod is a typical electrical dipole. The dipole moment is reduced in crooked nanoantennas, indicating a smaller radiative loss. In terms of the third-order mode, the nanorod consists of three electrical dipoles with the opposite directions. As a result, the net dipole moment of the third-order mode is smaller than the first-order mode, and the situation becomes more complicated in crooked nanoantennas. By folding the nanoantennas, the net dipole moment will first increase as in S4 but then decrease fast as in S8. As a result, the largest extinction is achieved when the nanoantennas are modestly crooked (S6), but the extinction becomes close to zero for severely crooked nanoantennas (S7 and S8). Besides, the relatively smaller net dipole moment in the higher-order mode leads to reduced radiative losses, resulting in higher quality (Q) factors, as shown in Figure 5c. From the graph, we can see that the Q-factors of the third-order modes are usually above 10, with a peak value of 20 in S6. In contrast, the Q-factors of the first-order modes are usually only a few.

The high-Q third order resonance modes in the crooked nanoantennas can be used for sensitive refractive index sensing, which is complementary to the absorption-based molecule sensing. As shown in Figure 5d, we simulate the transmission spectra of crooked nanoantennas (S6) with and without being coated with analytes. The analytes are modeled with a Lorentzian oscillator with its complex relative permittivity as a function of resonance frequency (f)

$$\varepsilon(f) = \varepsilon_0 + \frac{\varepsilon_{\text{lorentz}} \cdot \omega_0^2}{\omega_0^2 - 4\pi i \delta_0 f - (2\pi f)^2} \tag{12}$$

where background permittivity (ε_0), Lorentz permittivity ($\varepsilon_{\text{lorentz}}$), Lorentz resonance ($\omega_0$), and Lorentz linewidth (δ_0) are set to be 1.1, 0.002, 3.25×10^{14} rad s^{-1}, and 1.5×10^{12} rad s^{-1}, respectively. As we expected, there is a transmission peak around 6 μm due to the plasmon−molecule interaction. Besides, we also observe a resonance shift of the third-order mode around 2.5 μm. This occurs because the background permittivity is larger than 1, which is the relative permittivity of air. The sensitivity of the third-order mode can be estimated to be 920 nm RIU^{-1}. We then also demonstrate experiments for PMMA and CO_2 sensing, as shown in Figure 5e,f. Similar results are observed as the simulation. Interestingly, our experiment also shows a resonance shift of about 10 nm when PEI is placed in 450 ppm CO_2. This could be because the existence of CO_2 molecules in PEI leads to more vibrational bonds that contribute to the background permittivity.[45] The change of the refractive index can be estimated to be about 0.011.

3. CONCLUSIONS

In conclusion, we have proposed crooked nanoantennas via loss engineering for ultrasensitive transmissive infrared spectroscopy. The enhancement factor achieved in crooked nanoantennas is up to 2.8×10^4, above one order higher than the value in conventional straight nanoantennas. Importantly, our structure excludes challenging nanogap fabrication, demonstrating loss engineering as a promising solution to overcome the current bottlenecks of nanoantenna molecule sensors. We also theoretically investigate and experimentally validate the different effects of spectral detuning on straight and crooked nanoantennas. Leveraging PEI as an enrichment layer, we also demonstrate a transmissive plasmonic CO_2 sensor based on optimized crooked nanoantennas with sensitivities up to 0.067% ppm^{-1}. Finally, we study the effect of loss engineering on the higher order of nanoantennas and present multiband plasmonic sensors to simultaneously detect the refractive index and characteristic absorption of molecules. The approach reported in this work is general and can be applied for designing other geometries, including waveguide-based systems.[46,47] The crooked nanoantennas can be mass-produced using commercial optical lithography, which is an important step toward practical applications of miniaturized infrared spectroscopy.

DOI: 10.1021/acsami.9b18002
ACS Appl. Mater. Interfaces 2019, 11, 47270−47278

4. METHODS

4.1. Numerical Simulation. The simulation was performed using a three-dimensional FDTD method (Lumerical Inc). In the simulation, the complex refractive index of Au from Palik et al. is used, and the refractive index of CaF_2 is set to 1.4 for all wavelengths. The thickness of the CaF_2 substrate is set to be infinite. Besides, the simulation was performed on a unit cell applied with periodic boundary conditions to boost the modeling efficiency.

4.2. Sample Fabrication. CaF_2 wafer was sonicated in acetone for 10 min and then rinsed in IPA, followed by nitrogen drying. After drying, the clean CaF_2 wafer was coated with a 220 nm thick layer of PMMA e-beam lithography resist. Since the CaF_2 substrate was insulating, a thin conducting polymer film ESpacer (Showa Denko Singapore) was spin-coated at a speed of 2000 rpm. After being exposed by E-beam Lithography (Jeol 6300-FS), the samples were first immersed in DI water to remove the ESpacer film, then developed in the mixture of MIBK/IPA (1:3) for 30 s, and finally rinsed in IPA for 30 s. Afterward, 5 nm Cr and 80 nm Au was deposited on the sample by thermal evaporation, followed by a lift-off process in acetone for 24 h. For demonstration with the PMMA thin film, 1% 495 K PMMA in anisole resist was spin-coated with 4000 rpm speed. As for CO_2 sensing, the PEI enrichment layer was first diluted in deionized water with a mass ratio of 1:10, and then spin-coated on samples at a speed of 4000 rpm. Before spin coating, CaF_2 samples were treated with oxygen plasma to make the surface more hydrophilic.

4.3. Infrared Spectrum Characterization. The infrared spectra of plasmonic sensors were characterized by a Fourier transform infrared microscope (Agilent Cary 610 Series). One polarizer was used to keep the polarization of incident light along the designed direction. For the CO_2 sensing measurement, a gas chamber integrated with a heating stage is used. The gas cell was first heated up to 70 °C and flowed with pure nitrogen to remove the remaining CO_2 inside. After 10 min, the heater was turned off, while the nitrogen flow was not off until the gas cell reached room temperature. Afterward, gases with different precalibrated CO_2 concentrations were flowed into the gas cell. Then, the measurement was conducted after about 1 min when the concentration of CO_2 in the gas cell is assumed to be stable.

ASSOCIATED CONTENT

Supporting Information

The Supporting Information is available free of charge at https://pubs.acs.org/doi/10.1021/acsami.9b18002.

Summary of previous work; geometries, near-field distribution, simulated spectra, *Q*-factors, and field enhancement of designed nanoantennas; extraction of radiative and absorptive losses; measurement of PMMA thickness using AFM; fitting of molecule signals versus spectral detuning; chemical reactions between CO_2 and PEI; dependence of transmission change on the concentration of CO_2 in air (PDF)

AUTHOR INFORMATION

Corresponding Authors

*E-mail: chengwei.qiu@nus.edu.sg (C.-W.Q.).
*E-mail: elelc@nus.edu.sg (C.L.).

ORCID

Jingxuan Wei: 0000-0003-0295-3764
Yuhua Chang: 0000-0003-0337-1934
Chengkuo Lee: 0000-0002-8886-3649

Author Contributions

‖J.W. and Y.L. contributed equally to this work.

Notes

The authors declare no competing financial interest.

ACKNOWLEDGMENTS

This work was supported by the NRF CRP (No. R-263-000-C24-281), the NRF-ISF (No. R-263-000-C64-281) at the National University of Singapore, Singapore.

REFERENCES

(1) Griffiths, P. R.; De Haseth, J. A. *Fourier Transform Infrared Spectrometry*; Wiley-Interscience, 2007.
(2) Yang, X.; Sun, Z.; Low, T.; Hu, H.; Guo, X.; García de Abajo, F. J.; Avouris, P.; Dai, Q. Nanomaterial-Based Plasmon-Enhanced Infrared Spectroscopy. *Adv. Mater.* **2018**, *30*, 1−23.
(3) Neubrech, F.; Huck, C.; Weber, K.; Pucci, A.; Giessen, H. Surface-Enhanced Infrared Spectroscopy Using Resonant Nanoantennas. *Chem. Rev.* **2017**, *117*, 5110−5145.
(4) Fusco, Z.; Rahmani, M.; Bo, R.; Verre, R.; Motta, N.; Käll, M.; Neshev, D.; Tricoli, A. Nanostructured Dielectric Fractals on Resonant Plasmonic Metasurfaces for Selective and Sensitive Optical Sensing of Volatile Compounds. *Adv. Mater.* **2018**, *30*, No. 1800931.
(5) Liu, B.; Chen, S.; Zhang, J.; Yao, X.; Zhong, J.; Lin, H.; Huang, T.; Yang, Z.; Zhu, J.; Liu, S.; Lienau, C.; Wang, L.; Ren, B. A Plasmonic Sensor Array with Ultrahigh Figures of Merit and Resonance Linewidths down to 3 Nm. *Adv. Mater.* **2018**, *30*, No. e1706031.
(6) Rodrigo, D.; Tittl, A.; Ait-Bouziad, N.; John-Herpin, A.; Limaj, O.; Kelly, C.; Yoo, D.; Wittenberg, N. J.; Oh, S.; Lashuel, H. A.; Altug, H. Resolving Molecule-Specific Information in Dynamic Lipid Membrane Processes with Multi-Resonant Infrared Metasurfaces. *Nat. Commun.* **2018**, *9*, No. 2160.
(7) Zeng, S.; Sreekanth, K. V.; Shang, J.; Yu, T.; Chen, C. K.; Yin, F.; Baillargeat, D.; Coquet, P.; Ho, H. P.; Kabashin, A. V.; Yong, K. T. Graphene-Gold Metasurface Architectures for Ultrasensitive Plasmonic Biosensing. *Adv. Mater.* **2015**, *27*, 6163−6169.
(8) Dayal, G.; Chin, X. Y.; Soci, C.; Singh, R. High-Q Plasmonic Fano Resonance for Multiband Surface-Enhanced Infrared Absorption of Molecular Vibrational Sensing. *Adv. Opt. Mater.* **2017**, *5*, No. 1600559.
(9) Cubukcu, E.; Zhang, S.; Park, Y. S.; Bartal, G.; Zhang, X. Split Ring Resonator Sensors for Infrared Detection of Single Molecular Monolayers. *Appl. Phys. Lett.* **2009**, *95*, 1−4.
(10) Adato, R.; Yanik, A. A.; Amsden, J. J.; Kaplan, D. L.; Omenetto, F. G.; Hong, M. K.; Erramilli, S.; Altug, H. Ultra-Sensitive Vibrational Spectroscopy of Protein Monolayers with Plasmonic Nanoantenna Arrays. *Proc. Natl. Acad. Sci. U.S.A.* **2009**, *106*, 19227−19232.
(11) Wu, C.; Khanikaev, A. B.; Adato, R.; Arju, N.; Yanik, A. A.; Altug, H.; Shvets, G. Fano-Resonant Asymmetric Metamaterials for Ultrasensitive Spectroscopy and Identification of Molecular Monolayers. *Nat. Mater.* **2012**, *11*, 69−75.
(12) Brown, L. V.; Yang, X.; Zhao, K.; Zheng, B. Y.; Nordlander, P.; Halas, N. J. Fan-Shaped Gold Nanoantennas above Reflective Substrates for Surface-Enhanced Infrared Absorption (SEIRA). *Nano Lett.* **2015**, *15*, 1272−1280.
(13) Huck, C.; Vogt, J.; Sendner, M.; Hengstler, D.; Neubrech, F.; Pucci, A. Plasmonic Enhancement of Infrared Vibrational Signals: Nanoslits versus Nanorods. *ACS Photonics* **2015**, *2*, 1489−1497.
(14) Cerjan, B.; Yang, X.; Nordlander, P.; Halas, N. J. Asymmetric Aluminum Antennas for Self-Calibrating Surface-Enhanced Infrared Absorption Spectroscopy. *ACS Photonics* **2016**, *3*, 354−360.
(15) Vogt, J.; Zimmermann, S.; Huck, C.; Tzschoppe, M.; Neubrech, F.; Fatikow, S.; Pucci, A. Chemical Identification of Individual Fine Dust Particles with Resonant Plasmonic Enhancement of Nanoslits in the Infrared. *ACS Photonics* **2017**, *4*, 560−566.
(16) Chen, X.; Wang, C.; Yao, Y.; Wang, C. Plasmonic Vertically Coupled Complementary Antennas for Dual-Mode Infrared Molecule Sensing. *ACS Nano* **2017**, *11*, 8034−8046.
(17) Kühner, L.; Hentschel, M.; Zschieschang, U.; Klauk, H.; Vogt, J.; Huck, C.; Giessen, H.; Neubrech, F. Nanoantenna-Enhanced Infrared Spectroscopic Chemical Imaging. *ACS Sensors* **2017**, *2*, 655−662.

DOI: 10.1021/acsami.9b18002
ACS Appl. Mater. Interfaces 2019, 11, 47270−47278

(18) Adato, R.; Altug, H. In-Situ Ultra-Sensitive Infrared Absorption Spectroscopy of Biomolecule Interactions in Real Time with Plasmonic Nanoantennas. *Nat. Commun.* **2013**, *4*, No. 2154.
(19) Limaj, O.; Etezadi, D.; Wittenberg, N. J.; Rodrigo, D.; Yoo, D.; Oh, S. H.; Altug, H. Infrared Plasmonic Biosensor for Real-Time and Label-Free Monitoring of Lipid Membranes. *Nano Lett.* **2016**, *16*, 1502−1508.
(20) Semenyshyn, R.; Hentschel, M.; Stanglmair, C.; Teutsch, T.; Tarin, C.; Pacholski, C.; Giessen, H.; Neubrech, F. In Vitro Monitoring Conformational Changes of Polypeptide Monolayers Using Infrared Plasmonic Nanoantennas. *Nano Lett.* **2019**, *19*, 1−7.
(21) Huck, C.; Tzschoppe, M.; Semenyshyn, R.; Neubrech, F.; Pucci, A. Chemical Identification of Single Ultrafine Particles Using Surface-Enhanced Infrared Absorption. *Phys. Rev. Appl.* **2019**, *11*, No. 014036.
(22) Chen, C.; Mohr, D. A.; Choi, H. K.; Yoo, D.; Li, M.; Oh, S. H. Waveguide-Integrated Compact Plasmonic Resonators for On-Chip Mid-Infrared Laser Spectroscopy. *Nano Lett.* **2018**, *18*, 7601−7608.
(23) Mohr, D. A.; Nguyen, N.-C.; Peraire, J.; Yoo, D.; Caldwell, J. D.; Jo, M.; Kim, S.; Martin-Moreno, L.; Altug, H.; Jeon, H.; Matson, J.; John-Herpin, A.; Oh, S.-H.; Vidal-Codina, F. High-Contrast Infrared Absorption Spectroscopy via Mass-Produced Coaxial Zero-Mode Resonators with Sub-10 nm Gaps. *Nano Lett.* **2018**, *18*, 1930−1936.
(24) Aizpurua, J.; Bryant, G. W.; Richter, L. J.; García de Abajo, F. J.; Kelley, B. K.; Mallouk, T. Optical Properties of Coupled Metallic Nanorods for Field-Enhanced Spectroscopy. *Phys. Rev. B* **2005**, *71*, No. 235420.
(25) Dong, L.; Yang, X.; Zhang, C.; Cerjan, B.; Zhou, L.; Tseng, M. L.; Zhang, Y.; Alabastri, A.; Nordlander, P.; Halas, N. J. Nanogapped Au Antennas for Ultrasensitive Surface-Enhanced Infrared Absorption Spectroscopy. *Nano Lett.* **2017**, *17*, 5768−5774.
(26) Le, T. H. H.; Tanaka, T. Plasmonics-Nanofluidics Hydrid Metamaterial: An Ultrasensitive Platform for Infrared Absorption Spectroscopy and Quantitative Measurement of Molecules. *ACS Nano* **2017**, *11*, 9780−9788.
(27) Hwang, I.; Yu, J.; Lee, J.; Choi, J.-H.; Choi, D.-G.; Jeon, S.; Lee, J.; Jung, J.-Y. Plasmon-Enhanced Infrared Spectroscopy Based on Metamaterial Absorbers with Dielectric Nanopedestals. *ACS Photonics* **2018**, *5*, 3492−3498.
(28) Cong, L.; Pitchappa, P.; Lee, C.; Singh, R. Active Phase Transition via Loss Engineering in a Terahertz MEMS Metamaterial. *Adv. Mater.* **2017**, *29*, 1−7.
(29) Verslegers, L.; Yu, Z.; Ruan, Z.; Catrysse, P. B.; Fan, S. From Electromagnetically Induced Transparency to Superscattering with a Single Structure: A Coupled-Mode Theory for Doubly Resonant Structures. *Phys. Rev. Lett.* **2012**, *108*, 1−5.
(30) Adato, R.; Artar, A.; Erramilli, S.; Altug, H. Engineered Absorption Enhancement and Induced Transparency in Coupled Molecular and Plasmonic Resonator Systems. *Nano Lett.* **2013**, *13*, 2584−2591.
(31) Gallinet, B.; Martin, O. J. F. Refractive Index Sensing with Subradiant Modes: A Framework to Reduce Losses in Plasmonic Nanostructures. *ACS Nano* **2013**, *7*, 6978−6987.
(32) Neuman, T.; Huck, C.; Vogt, J.; Neubrech, F.; Hillenbrand, R.; Aizpurua, J.; Pucci, A. Importance of Plasmonic Scattering for an Optimal Enhancement of Vibrational Absorption in SEIRA with Linear Metallic Antennas. *J. Phys. Chem. C* **2015**, *119*, 26652−26662.
(33) Haus, H. A. *Waves and Fields in Optoelectronics*; Prentice-Hall: NJ, 1984.
(34) Adato, R.; Yanik, A. A.; Altug, H. On Chip Plasmonic Monopole Nano-Antennas and Circuits. *Nano Lett.* **2011**, *11*, 5219−5226.
(35) Hasan, D.; Pitchappa, P.; Wang, J.; Wang, T.; Yang, B.; Ho, C. P.; Lee, C. Novel CMOS-Compatible Mo−AlN−Mo Platform for Metamaterial-Based Mid-IR Absorber. *ACS Photonics* **2017**, *4*, 302−315.
(36) Hasan, D.; Pitchappa, P.; Pei Ho, C.; Lee, C. High Temperature Coupling of IR Inactive C=C Mode in Complementary Metal Oxide Semiconductor Metamaterial Structure. *Adv. Opt. Mater.* **2017**, *5*, No. 1600778.
(37) Giannini, V.; Francescato, Y.; Amrania, H.; Phillips, C. C.; Maier, S. A. Fano Resonances in Nanoscale Plasmonic Systems: A Parameter-Free Modeling Approach. *Nano Lett.* **2011**, *11*, 2835−2840.
(38) Osley, E. J.; Biris, C. G.; Thompson, P. G.; Jahromi, R. R. F.; Warburton, P. A.; Panoiu, N. C. Fano Resonance Resulting from a Tunable Interaction between Molecular Vibrational Modes and a Double Continuum of a Plasmonic Metamolecule. *Phys. Rev. Lett.* **2013**, *110*, 1−5.
(39) Alonso-González, P.; Albella, P.; Neubrech, F.; Huck, C.; Chen, J.; Golmar, F.; Casanova, F.; Hueso, L. E.; Pucci, A.; Aizpurua, J.; Hillenbrand, R. Experimental Verification of the Spectral Shift between Near- and Far-Field Peak Intensities of Plasmonic Infrared Nanoantennas. *Phys. Rev. Lett.* **2013**, *110*, 1−6.
(40) Hasan, D.; Lee, C. Hybrid Metamaterial Absorber Platform for Sensing of CO_2 Gas at Mid-IR. *Adv. Sci.* **2018**, *5*, No. 1700581.
(41) Chang, Y.; Hasan, D.; Dong, B.; Wei, J.; Ma, Y.; Zhou, G.; Ang, K. W.; Lee, C. All-Dielectric Surface-Enhanced Infrared Absorption-Based Gas Sensor Using Guided Resonance. *ACS Appl. Mater. Interfaces* **2018**, *10*, 38272−38279.
(42) Hahn, M. W.; Steib, M.; Jentys, A.; Lercher, J. A. Mechanism and Kinetics of CO2adsorption on Surface Bonded Amines. *J. Phys. Chem. C* **2015**, *119*, 4126−4135.
(43) Moumen, S.; Raible, I.; Krauß, A.; Wöllenstein, J. Infrared Investigation of CO_2 sorption by Amine Based Materials for the Development of a NDIR CO_2 sensor. *Sens. Actuators, B* **2016**, *236*, 1083−1090.
(44) Chen, K.; Adato, R.; Altug, H. Dual-Band Perfect Absorber for Infrared Spectroscopy. *ACS Nano* **2012**, *6*, 7998−8006.
(45) Fox, M.; et al. Optical Properties of Solids. *Am. J. Phys.* **2002**, *70*, 1269−1270.
(46) Sun, F.; Wei, J.; Dong, B.; Ma, Y.; Chang, Y.; Tian, H.; Lee, C. Coexistence of Air and Dielectric Modes in Single Nanocavity. *Opt. Express* **2019**, *27*, No. 14085.
(47) Wei, J.; Sun, F.; Dong, B.; Ma, Y.; Chang, Y.; Tian, H.; Lee, C. Deterministic Aperiodic Photonic Crystal Nanobeam Supporting Adjustable Multiple Mode-Matched Resonances. *Opt. Lett.* **2018**, *43*, No. 5407.

DOI: 10.1021/acsami.9b18002
ACS Appl. Mater. Interfaces 2019, 11, 47270−47278